Available online at www.sciencedirect.com
SCIENCE DIRECT®
Journal of Nuclear Materials 337–339 (2005) 10–16
journal of nuclear materials
www.elsevier.com/locate/jnucmat

Tungsten redistribution patterns in ASDEX Upgrade

K. Krieger [a,*], J. Likonen [b], M. Mayer [a], R. Pugno [a], V. Rohde [a], E. Vainonen-Ahlgren [b], ASDEX Upgrade Team

[a] *MPI für Plasmaphysik, EURATOM Association, D-85748 Garching, Germany*
[b] *Association EURATOM-TEKES, VTT Processes, P.O. Box 1608, 02044 VTT, Finland*

Abstract

In ASDEX Upgrade tungsten is used as a high-Z plasma facing material. Its erosion, migration and subsequent deposition have been studied by analysis of a set of customised marker tiles, which was installed in the divertor and at the central column for one experimental campaign. Erosion rates were determined at the central column, which was the main tungsten source in that campaign. Deposition rates were determined at the central column and in the divertor region. The W-deposition in the divertor is strongly correlated to the local strike point exposure time. In contrast to low-Z wall materials, where deposition occurs mainly in the inner divertor, tungsten is found in similar quantities also in the outer divertor. The total amount of tungsten deposited outside the central column is about 40% of the gross W-source at the central column. One possible explanation for the 60% undetected tungsten might be the prompt local redeposition of eroded W atoms.

PACS: 28.52.Fa; 52.25.Vy; 52.40.Hf
Keywords: ASDEX Upgrade; Erosion and deposition; First wall; Impurity transport; Tungsten

1. Introduction

In ASDEX Upgrade tungsten is used as plasma facing material, replacing increasing fractions of the original carbon based wall components. The tungsten surface is to some extent eroded by impact of plasma ions. The eroded atoms will be ionised and will migrate through the plasma boundary and, in a smaller fraction, through the confined plasma, until they are finally redeposited at other locations in contact with the plasma. To assess aspects like lifetime of plasma facing materials, plasma impurity content and material mixing processes, it is necessary to study these processes in detail, particularly with respect to the extrapolation and model validation requirements for future fusion devices.

Erosion fluxes of wall material can be quantified by exposure of thin layers whose change in thickness can be determined very accurately by ion beam analysis methods. Ion beam analysis of retrieved material collection samples is also the only suitable method to quantify the deposition flux of an element. Retrieved tiles had been analysed already after previous campaigns [1] but the interpretation of the results was hampered by the fact that there was no consistent set of samples exposed in the same experimental campaign.

Therefore, in experimental campaign 2002–2003, a customised set of tiles with erosion markers was installed

* Corresponding author. Tel.: +49 89 3299 1655; fax: +49 89 3299 2279.
E-mail address: krieger@ipp.mpg.de (K. Krieger).

0022-3115/$ - see front matter © 2004 Elsevier B.V. All rights reserved.
doi:10.1016/j.jnucmat.2004.09.044

both in the lower divertor of the machine as well as at the central column.

2. Experimental set-up

The tungsten plasma facing surfaces in the campaign 2002–2003 consisted of the entire inner column (denoted W_1), the inner divertor baffle (W_2) and, at the low field side, the tiles covering the upper passive stabilisation coil (PSL, W_3) as shown schematically in Fig. 1. The tungsten components were manufactured by applying a 1 μm PVD coating on graphite tiles [2]. The total area (14.6 m^2) of the W-coated tiles was 40% of the total surface of plasma facing components, with 8.1 m^2 of W-coated tiles at the central column, 1.5 m^2 at the inner divertor baffle and 5.0 m^2 PSL tiles.

The tiles equipped with dedicated markers are shown in Fig. 1 with filled outlines. Of such tiles two different sets were installed at the central column and the divertor respectively. For the central column, metallic marker stripes were prepared along the toroidal coordinate on uncoated polished graphite tiles. At three poloidal positions at the upper and lower edge of the central column and at the midplane position, one tile was installed with marker stripes of molybdenum and tungsten and another tile at the adjacent toroidal segment with markers made of nickel. For each element, two markers were prepared at the upper and lower half of the tiles. In the divertor, a carbon layer was prepared on a complete cross-section of tiles by magnetron sputtering. To allow separation of the carbon layer from the carbon substrate by ion beam analysis, a rhenium interlayer was used as a depth marker [3].

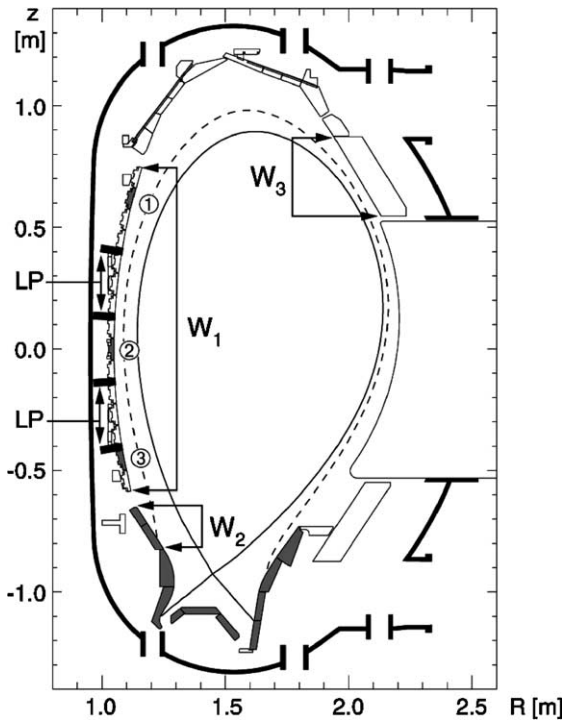

Fig. 1. Cross-section of the ASDEX Upgrade vacuum vessel with tungsten plasma facing components in experimental campaign 2002/2003. Installed diagnostic tile sets are shown in grey shade. The four central column Langmuir probes are denoted by LS.

Before installation in ASDEX Upgrade the markers were characterised by Rutherford backscattering (RBS) using protons in the energy range from 1.6 to 2.5 MeV. The area density of the marker material was derived from the RBS results by fitting a given layer structure to the measured spectra using the SIMNRA program [4]. In cases where a detailed depth profile was required, the program NDF [5] was used, which solves the inverse problem of extracting the depth distribution of elements from a Rutherford backscattering spectrum by a simulated annealing algorithm.

During the experimental campaign the tiles were exposed to 1205 plasma discharges with a total discharge time (determined as time where $I_p > 300$ kA) of 5973 s. For the calculation of average erosion rates, the integral erosion of the marker samples is divided by this time. To obtain average deposition rates in the divertor, only the plasma operation time with divertor plasma exposure (4934 s) is taken into account.

After the experimental campaign the retrieved tiles were again analysed by proton RBS to determine the thickness change of the markers and by PIXE to quantify the amount of deposited tungsten.

3. Tungsten erosion measurements

3.1. Campaign integrated erosion of tungsten markers

The measured W-layer erosion at the three marker tile positions is shown in Fig. 2. The pronounced toroidal asymmetry at the midplane position and at the lower edge of the central column is a result of the field line intersection geometry with the surface of the tiles. Depending on the inclination angle of the *B* field against the tile surface, the incident ion flux will be either shadowed or elevated. A similar behaviour was already observed at marker tiles installed during the experimental campaign 2001. In this case, the erosion was, however, measured only at one half of a toroidal segment with the tile surface oriented in a way that the maximum observed erosion was found at the upper half of the central column [1].

For the marker tile at the top of the central column, the erosion is below the detection limit because of the limited contact with the plasma. Average erosion rates

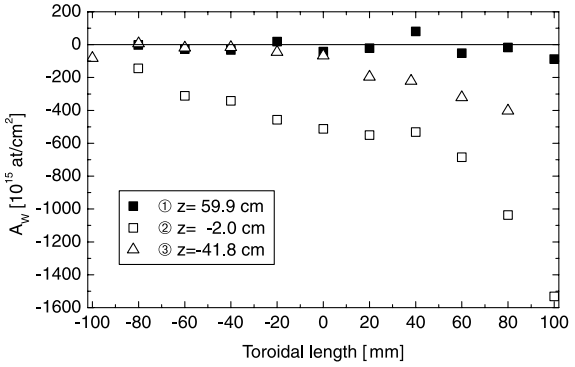

Fig. 2. Toroidal distribution of W-marker erosion at central column tiles. The z-positions of the markers are relative to the vessel midplane with tile position numbers as shown in Fig. 1.

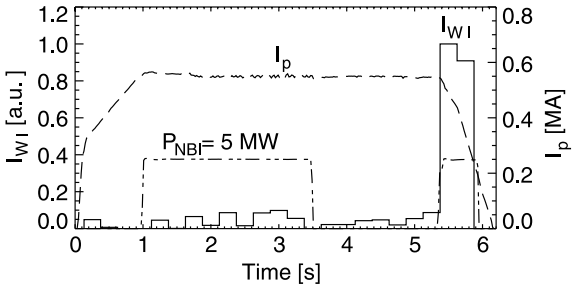

Fig. 3. Time evolution of spectroscopically measured W I line intensity at central column 4.2 cm above the midplane in H-mode discharge 16702. Also shown are the time traces of plasma current and neutral beam heating power.

for the two other tile positions are 54 nm/h at the midplane and 11 nm/h at the lower edge of the central column. These results are comparable to those measured for the previously (2001/2002) installed tiles with facetted surfaces [1].

Because W-marker tiles could be installed only at three poloidal positions, the total tungsten source derived from these measurements is just an estimate with a large experimental error. By integrating over the toroidal and poloidal distribution of the W-erosion measured at the facetted marker tiles in experiment campaign 2001/2002 [1] the average W-source was determined to $3.4 \times 10^{18}\ s^{-1}$. For the calculation the toroidal variation along the tile was considered to repeat itself around the central column. Assuming that the relative poloidal variation of the tile erosion at the central column did not change significantly by the transition from facetted to rounded tile surfaces, one can repeat this calculation for the tiles from campaign 2002/2003 using the previously measured shape of the poloidal distribution for interpolation between the tiles and obtain a quite similar total source rate of $3.1 \times 10^{18}\ s^{-1}$ for the central column.

Similar erosion rates to those at the lower part of the central column were also obtained from marker erosion measurements at the low field side in the experimental campaign 2002 [6] whereas at the inner divertor baffle tiles in the same campaign W-erosion was negligible [6]. Assuming the same erosion rate as from the markers exposed in the previous campaign at the upper passive stabilisation coil (PSL) protection tiles [6], we obtain for campaign 2002/2003 an additional W-source rate at the low field side of $1 \times 10^{18}\ s^{-1}$.

3.2. Spectroscopic measurement of the W-erosion flux

Since the marker erosion measurements reflect integrals over a full experimental campaign, time resolved measurements are necessary to determine which fractions of the integral value can be attributed to different discharge conditions. Spectroscopic detection of W I line radiation in the visible range at 400.8 nm had been used already in the ASDEX Upgrade tungsten divertor experiment [7]. For measurements at the central column a system with 10 fibre guides was installed [8].

Absolute calibration of spectroscopic data was not yet available in campaign 2002/2003 and therefore no erosion fluxes could be derived from the W I signal. The intensity of the W I line can be used, however, to identify plasma regimes with increased erosion flux. As an example the time evolution of the W I emission near the midplane position is shown in Fig. 3 together with plasma current and neutral beam heating power for a stationary low density H-mode discharge with medium triangularity plasma. During the flat top plasma phase the W I signal does not rise significantly above the system noise level. Only during plasma ramp-down, the emission is intense enough to derive the W I line intensity from the recorded spectra. Langmuir probe measurements of the local electron density and temperature show that this is due to the strongly elevated incident particle flux during this phase where the plasma column is leaning against the inner wall [9]. Since the W-erosion derived from the local plasma parameters using known W-sputtering yields described the spectroscopically measured W-fluxes fairly well in single discharges [9], it is justified to derive the campaign integrated W-erosion from the Langmuir probe data for comparison with the marker erosion results.

3.3. Derivation of W-erosion rates from local Langmuir probe data

For measurements of the local electron temperature and ion fluxes at the central column, an array of Langmuir probes was installed as shown in Fig. 1. The probes were active in 759 of the 1205 discharges of that campaign. Using the probe data, the local W-erosion flux $\Gamma_W = \Gamma_D \times Y_{eff}(T_e)$ can be calculated and integrated

over all available discharges. For the calculation, the effective tungsten sputtering yield, including the sputtering of tungsten by light plasma impurities, must be known as a function of T_e. For the analysis spectroscopically measured W-sputtering yields from the ASDEX Upgrade tungsten divertor experiment were used [7]. The resulting erosion agrees very well with values obtained using W-sputtering yields from TRIM simulations [10], assuming sputtering by deuterium and a 1% fraction of C^{2+} ions as substitute for the low-Z impurity ions incident at the central column. The Langmuir probes installed at the central column consist of graphite pins protruding a few mm above the tile surface. To derive the ion flux at the tile surface from the detected parallel particle flux, one needs to calculate the projection of the incident field lines on the tile surfaces. In principle it is possible to derive the local inclination angles from the magnetic field reconstruction to take into account the shape of the tiles. For this analysis a simplified approach was used, assuming a tile surface averaged inclination angle of 1°. The campaign integrated erosion was calculated separately for limiter and divertor plasma configurations. Each value was in addition scaled with the ratio of total discharge time over total probe activation time in that particular plasma configuration. The results are shown in Fig. 4. The calculated erosion during the stationary divertor phases is mainly located at the lower half of the central column. This is in agreement with spectroscopic measurements of carbon and deuterium fluxes at the central column, which also show a strong increase of D recycling flux and C influx towards the lower edge of the central column [11]. In the limiter phase the erosion pattern has no pronounced maximum. The erosion minimum just above the midplane can be attributed to the almost tangential B field and correspondingly strongly decreased particle flux to the probe. This was confirmed in discharges where the spatial resolution of the Langmuir probes was enhanced by vertical sweeps of the plasma column. The profiles of the electron density show indeed a strong decrease between $z = 0$ and 0.1 m [12].

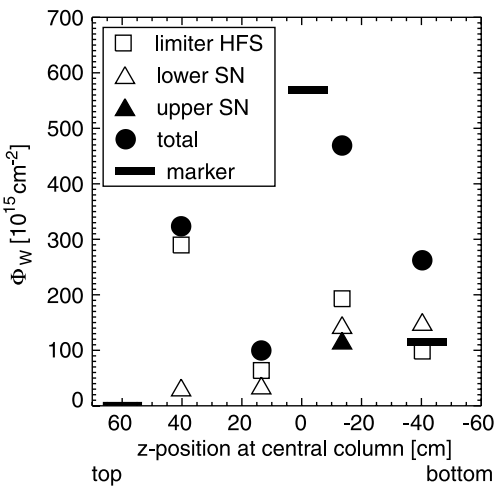

Fig. 4. Campaign integral of W-erosion calculated from Langmuir probe data. The open triangles and squares refer to the eroded fractions during single null lower divertor (lower SN) and inner wall limiter (limiter HFS). The bars represent the average tile erosion measured at the marker tiles (Fig. 2).

Table 1
Average tungsten source rates from different experimental methods

Central column markers 2001/2002	3.4×10^{18} s^{-1}
Central column markers 2002/2003	3.1×10^{18} s^{-1}
Central column Langmuir probes 2002/2003	3.9×10^{18} s^{-1}
Passive stabiliser coil tiles 2002/2003 [6]	1×10^{18} s^{-1}

By taking the spatial average of the W-erosion campaign integrals derived from the Langmuir probe data, one can calculate an estimate for the average total source rate of tungsten in campaign 2002/2003 and obtains a value of 3.9×10^{18} s^{-1} with an approximately 1/3 contribution from the flattop single null configuration and 2/3 from the central column limiter configuration. Source rates obtained from the different experimental approaches are summarised in Table 1. For a direct comparison of the data one should take into account that the measured marker erosion might be smaller than the actual gross erosion rate due to W-redeposition. Furthermore, one has to consider that the erosion rate calculated from the Langmuir probe data is mainly determined by the assumed effective sputtering yield and angle of incidence. The effective sputtering yield is in turn strongly depending on the concentration of low-Z impurities in the boundary plasma, which is not exactly known.

4. Tungsten deposition measurements

4.1. Tungsten deposition in the divertor

Tungsten deposition in the divertor was measured on the carbon tiles with C/Re marker stripes by PIXE analysis of the uncoated surface area beside the markers. SIMS depth profiling showed that particularly at the strike point tiles, light elements (B, C) have been deposited with a thickness up to several microns [13]. Therefore, PIXE analysis at these tiles was performed with 2.5 MeV protons, which allows to detect tungsten from the surface to a depth of approximately 30 μm. The resulting poloidal W-deposition pattern along the tile surface length is shown in Fig. 5. At the strike point tiles the amount of deposited tungsten is strongly correlated to the integrated strike point exposure time, which

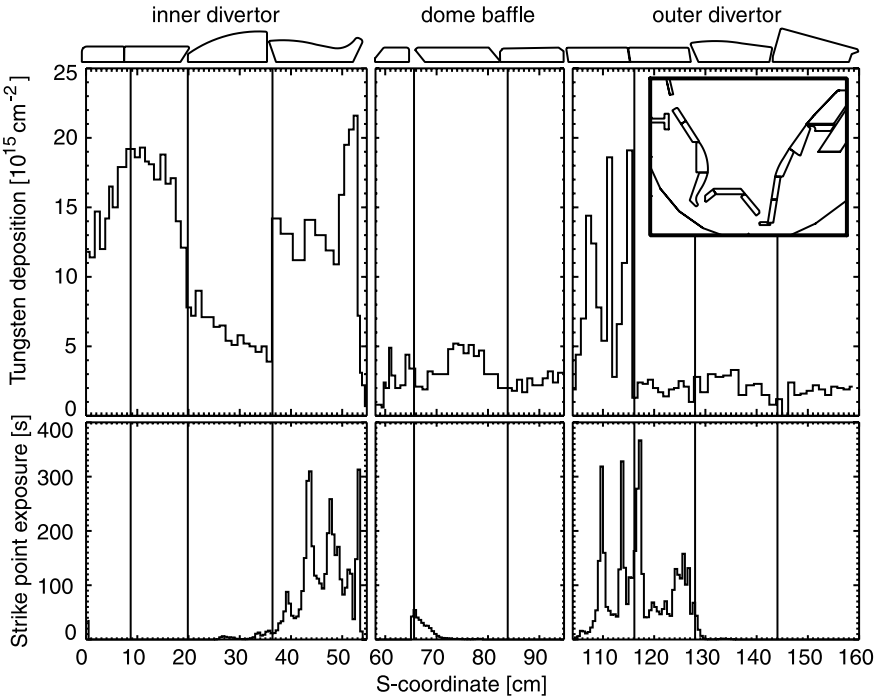

Fig. 5. Tungsten deposition in the lower divertor of ASDEX Upgrade after campaign 2002/2003. The data are plotted as a function of the poloidal path length along the tile surface. The lower plot shows the integrated strike point exposure time of the tile surface.

indicates that the tungsten deposited in these zones has been transported into the divertor through the near-separatrix boundary plasma. One finds also that tungsten is deposited in similar fractions both in the inner and the outer divertor: the W-deposition rate integrated over the strike point wetted zone of the outer divertor is $4.1 \times 10^{16}\,s^{-1}$ and at the inner divertor $3.1 \times 10^{16}\,s^{-1}$. This is a striking difference to the behaviour of low-Z impurities, where deposition is practically only found in the inner divertor [3,14], while the outer divertor is dominated by erosion. A possible explanation is the much smaller re-erosion of deposited tungsten as opposed to that of lighter elements. The absence of significant low-Z deposits at the outboard divertor found in many tokamaks could be a result not only of scrape-off layer flows predominantly directed to the inboard side [15–17] but also of the continuous re-erosion of light elements, which prevents formation of large deposits.

Similar to previous measurements [1] there is also comparatively high deposition of tungsten at the inboard baffle region. This is a result of the direct connection of this zone along the magnetic field to the tungsten covered lower part of the central column [18].

By integrating the total W-deposition in the inner and outer divertor and baffle regions one obtains a campaign averaged total W-sink rate of $1.1 \times 10^{17}\,s^{-1}$ for the inboard side and $0.5 \times 10^{17}\,s^{-1}$ for the outboard side of the divertor. The total W-divertor sink is much smaller than the total W-source (Section 3) and the question remains where the main fraction of eroded tungsten is migrating. The deposition rate to the divertor strike point zones is, however, close to the rate of tungsten penetrating the plasma during divertor operation, assuming a penetration probability of 4% as measured before by laser ablation [19]. This indicates that the main fraction of eroded tungsten must have been redeposited locally.

4.2. Tungsten redeposition at the central column

As was done for the divertor tiles, the amount of redeposited tungsten at the central column tiles was measured by PIXE analysis and in addition at some positions with RBS. From the RBS spectra the depth distribution of the redeposited tungsten was reconstructed using the NDF code [5]. It turned out that the surface to a depth of ≈500 nm consists mainly of boron and silicon with the deposited tungsten embedded as a ≈1% fraction. Since the thickness of the boron and silicon layers applied with glow discharge wall-conditioning is only in the range of a few 10 nm, this result must be interpreted as a consequence of the surface roughness of the tiles, which is in the 1 μm range. B, Si and also redeposited tungsten will normally be re-eroded because the central column is, as shown in Section 3, an erosion

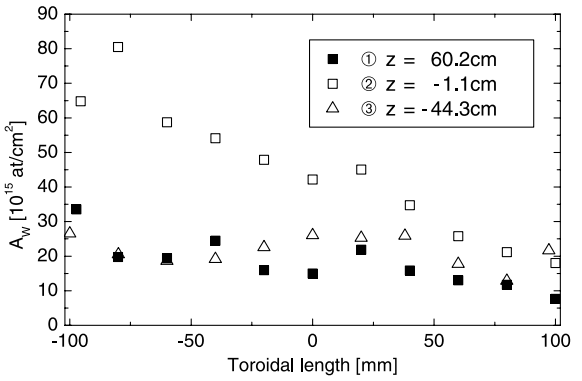

Fig. 6. Toroidal distribution of W-deposition at central column tiles. The z-positions of the markers are relative to the vessel midplane with tile position numbers as shown in Fig. 1.

dominated region, however, material deposited in pores and depressions of the rough surface is protected to some extent. The amount of deposited tungsten at the three poloidal marker tile positions is shown in Fig. 6. The toroidal distribution is anti-correlated to that of the tungsten erosion shown in Fig. 2. Comparison of W-deposition measurements at different poloidal distances from the tungsten markers show a decrease with increasing poloidal distance, which indicates prompt redeposition of W. For a quantitative determination of the promptly redeposited fraction further analysis of the deposition pattern perpendicular to the marker stripes will be necessary.

Taking the average tungsten deposition on the analysed tiles, one obtains a total campaign averaged sink rate at the central column itself of $3.8 \times 10^{17}\,s^{-1}$. This is, however, only a lower limit, because the transport length due to prompt redeposition is only a few mm [20] and therefore only a minor fraction of tungsten eroded at neighbouring tiles will actually reach the graphite marker tiles.

4.3. Deposition of tungsten at side faces of tiles

Recent experiments, for example at TEXTOR [21], have shown that not only carbon but also tungsten migrates to some extent into gaps between tiles or castellated structures. This possible migration channel was examined by analysing W-deposition at the side faces of the central column tiles, which are mounted with gaps of ≈4 mm in poloidal direction and with up to 10 mm in toroidal direction. The amount of deposited tungsten at the side faces decreases exponentially from the surface with fall-off lengths of 1.5–2.5 mm. If one integrates the deposition at all four tile side faces and assumes that deposition is the same for all 448 central column tiles, one obtains a total campaign averaged deposition rate of $0.7 \times 10^{17}\,s^{-1}$, which is slightly higher than the deposition in the outer divertor, but again only a minor fraction of the total W-gross erosion rate.

5. Migration pattern of tungsten

Taking all measured results of tungsten erosion and of deposition into account, it is possible to condense the data in a simple picture of the tungsten migration paths during the divertor phase and during the limiter phase respectively, as shown in Fig. 7. The separate consideration of both configurations is required because W-deposition in the divertor cannot originate from tungsten eroded during the limiter phases where there is no contact between plasma and divertor. For the limiter phase, the transport of eroded tungsten was modelled using the DIVIMP code with a plasma background created with B2/EIRENE [12]. The code predicts that nearly all eroded tungsten is redeposited back at the central column, which is the only surface with direct plasma contact in this configuration. Only a minor part (<10%)

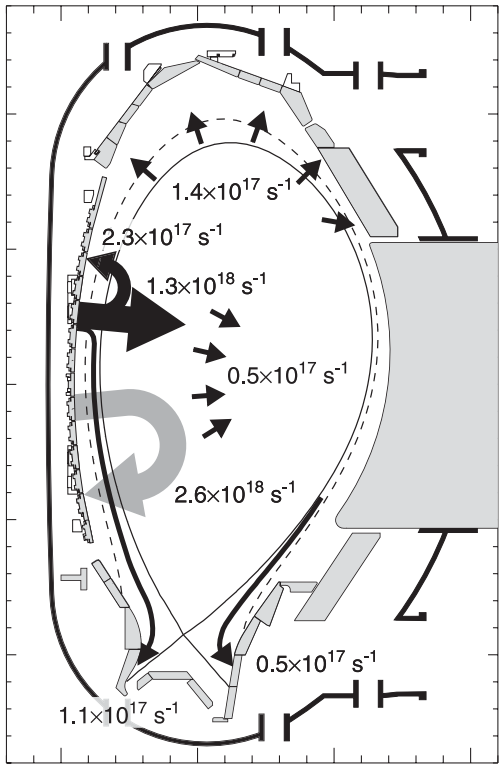

Fig. 7. Migration paths for tungsten. The black arrows and numbers denote tungsten source and sink rates in the lower divertor configuration, the grey arrows and numbers represent respective rates in the limiter phase. Only a 4% fraction of the eroded tungsten is actually entering the core plasma while the remaining fraction is returning to the plasma facing surfaces by transport processes in the edge plasma.

might end up at the low field side limiters. In divertor configuration, one concludes from the tungsten deposits found in the divertor that tungsten is migrating from the central column into the divertor, as shown in Fig. 7. One can add up all sinks in the divertor phase and balance these against the total source in that phase. For both erosion and deposition at the central column the total contributions were attributed to divertor and limiter phases according to their relative erosion fraction derived from the Langmuir probe data. For the divertor phase we obtain a total sink rate of $5.3 \times 10^{17}\ s^{-1}$ versus a total source rate of $1.3 \times 10^{18}\ s^{-1}$. Prompt redeposition, which is not accounted for in the data, might explain the difference although with the present experimental uncertainties the missing part could also be a result of measurement errors or of errors in the derivation of the integrated erosion from Langmuir probe data. Finally, it should be noted that the redeposition measured at the central column represents only a lower limit. More detailed mapping of the marker redeposition will help to clarify the discrepancy.

6. Summary

The mapping of the W-erosion and redistribution pattern indicates that only a minor fraction of the eroded tungsten is non-locally redeposited. Regions of non-local W-deposition are located at the baffle tiles of the inner divertor and at the strike point wetted zones both in the inner and outer divertor. W is migrating to the inboard baffle because of the direct connection with regions of the central column along magnetic field lines. In the divertor tungsten is deposited to almost equal fractions at the inner and outer target plates in amounts which are similar to that of tungsten predicted to penetrate into the core plasma. The quite even deposition in the inner and outer divertor is in contrast to that of light impurities [3,14], which are mainly deposited in the inner divertor.

The results show that tungsten eroded at main vessel wall surfaces will migrate to some extent into the divertor region although with respect to absolute amounts tungsten has a clear advantage over low-Z materials. Based on the results of ASDEX Upgrade the throughput of material by erosion and subsequent non-local redeposition is at least a factor of 100 smaller for tungsten compared to carbon. Similar results can be expected comparing tungsten to beryllium, which is foreseen as main chamber wall material in ITER. One has to relativise this conclusion, however, taking into account that the throughput of tungsten might significantly increase by its use as limiter material. First results from test limiter exposure at the plasma low-field side in ASDEX Upgrade show that in this case the tungsten erosion is an order of magnitude enhanced over the values observed at the central column [22].

References

[1] K. Krieger et al., J. Nucl. Mater. 313–316 (2003) 327.
[2] H. Maier et al., Surf. Coat. Technol. 142 (2001) 733.
[3] M. Mayer et al., Phys. Scr. T 111 (2004) 55.
[4] M. Mayer, in: 15th International Conference on the Application of Accelerators in Research and Industry, American Institute of Physics Conference Proceedings vol. 475, 1999, p. 541.
[5] N.P. Barradas, C. Jeynes, R.P. Webb, Appl. Phys. Lett. 71 (1997) 291.
[6] H. Maier et al., J. Nucl. Mater. 335 (2004) 515.
[7] A. Thoma et al., Plasma Phys. Control. Fusion 39 (1997) 1487.
[8] R. Neu et al., J. Nucl. Mater. 313–316 (2003) 116.
[9] V. Rohde et al., in: 18th IAEA Conference on Fusion Energy, Sorrento, Italy, IAEA-CN-77/EXP4/24, 2001.
[10] W. Eckstein et al., Sputtering data, IPP Report, MPI Plasmaphysik, IPP 9/82, 1993.
[11] T. Pütterich et al., Plasma Phys. Control. Fusion 45 (2003) 1873.
[12] A. Geier et al., Nucl. Fusion, submitted for publication.
[13] E. Vainonen-Ahlgren, these Proceedings. doi:10.1016/j.jnucmat.2004.08.028.
[14] G.F. Matthews et al., in: 30th EPS Conference on Contribution of Fusion and Plasma Physics, St. Petersburg, Europhysics Conference Abstracts 27A, P-3.198, 2003.
[15] N. Asakura et al., J. Nucl. Mater. 313–316 (2003) 820.
[16] S.K. Erents et al., Plasma Phys. Control. Fusion 42 (2000) 905.
[17] S. Gangadhara, B. LaBombard, J. Nucl. Mater. 313–316 (2003) 1167.
[18] K. Krieger et al., J. Nucl. Mater. 307–311 (2002) 139.
[19] R. Neu et al., J. Nucl. Mater. 290–293 (2001) 206.
[20] D. Naujoks et al., Nucl. Fusion 36 (1996) 671.
[21] P. Wienhold et al., J. Nucl. Mater. 313 (2003) 311.
[22] R. Dux, these Proceedings. doi:10.1016/j.jnucmat.2004.10.105.